Highly ABA-Induced 1 (HAI1)-Interacting protein HIN1 and drought acclimation-enhanced splicing efficiency at intron retention sites

Geeng Loo Chong[a,b,c], Mung Hsia Foo[a], Wen-Dar Lin[a], Min May Wong[a,b,c], and Paul E. Verslues[a,b,d,1]

[a]Institute of Plant and Microbial Biology, Academia Sinica, 115 Taipei, Taiwan; [b]Molecular and Biological Agricultural Sciences Program, Taiwan International Graduate Program, National Chung-Hsing University, 402 Taichung, Taiwan, and Academia Sinica, 115 Taipei, Taiwan; [c]Graduate Institute of Biotechnology, Biotechnology Center, National Chung-Hsing University, 402 Taichung, Taiwan; and [d]Biotechnology Center, National Chung-Hsing University, 402 Taichung, Taiwan

The Highly ABA-Induced 1 (HAI1) protein phosphatase is a central component of drought-related signaling. A screen for HAI1-interacting proteins identified HAI1-Interactor 1 (HIN1), a nuclear protein of unknown function which could be dephosphorylated by HAI1 in vitro. HIN1 colocalization and interaction with serine-arginine rich (SR) splicing factors and appearance of nuclear speckle-localized HIN1 during low water potential (ψ_w) stress suggested a pre-mRNA splicing-related function. RNA sequencing of *Arabidopsis* Col-0 wild type identified more than 500 introns where moderate severity low ψ_w altered intron retention (IR) frequency. Surprisingly, nearly 90% of these had increased splicing efficiency (decreased IR) during stress. For one-third of these introns, ectopic HIN1 expression (*35S:HIN1*) in unstressed plants mimicked the increased splicing efficiency seen in stress-treated wild type. HIN1 bound to a GAA-repeat, Exonic Splicing Enhancer-like RNA motif enriched in flanking sequence around HIN1-regulated introns. Genes with stress and HIN1-affected splicing efficiency were enriched for abiotic stress and signaling-related functions. The *35S:HIN1* plants had enhanced growth maintenance during low ψ_w, while *hin1* mutants had reduced growth, further indicating the role of HIN1 in drought response. HIN1 is annotated as an MYB/SANT domain protein but has limited homology to other MYB/SANT proteins and is not related to known yeast or metazoan RNA-binding proteins or splicing regulators. Together these data identify HIN1 as a plant-specific RNA-binding protein, show a specific effect of drought acclimation to promote splicing efficiency of IR-prone introns, and also discover HAI1–HIN1 interaction and dephosphorylation that connects stress signaling to splicing regulation.

alternative splicing | MYB/SANT domain | intron retention | *Arabidopsis thaliana* | HAI1 protein phosphatase

Limited water availability and low water potential (ψ_w) during drought cause extensive changes in plant gene regulation which in turn control physiological responses required for drought resistance. Alternative splicing of pre-mRNAs has emerged as an important layer of gene regulation responsive to abiotic stress (1–4). In pre-mRNA splicing, the 5′ end (donor site) of the intron forms a lariat structure with the branch point followed by removal of the intron at the 3′ acceptor site and exon ligation. For most introns, this process is highly efficient such that the intron is precisely removed to produce mature protein coding transcript. In other cases, the splicing process is more variable such that an intron may not always be removed (intron retention [IR]), alternative donor or acceptor sites may be used such that short sequences are added to or deleted from the mature mRNA, or an exon may be removed along with its flanking introns (exon skipping [ES]). In metazoans it is well established that alternative splicing is a regulated mechanism to produce multiple functionally distinct proteins from a single gene. This regulation is mediated, in part, by Exonic Splicing Enhancer (ESE) sequences that are adjacent to the exon–intron junction and influence splicing efficiency (3, 5–7).

ESE sequences are binding sites for splicing enhancer or repressor proteins that work with the core spliceosome components and other RNA-binding proteins to influence splicing efficiency or splice site selection. The mechanisms of splicing enhancer and repressor protein function remain incompletely known in any organism.

Plant alternative splicing has some key differences compared to metazoans. Notably, ES is less common in plants while IR is more common (8–10). As many IR events lead to frame shifts and introduction of premature stop codons (10) and IR transcripts may be less stable than fully spliced transcripts, plant alternative splicing appears to be more oriented toward controlling protein abundance rather than producing functionally distinct protein isoforms. However, cases where alternative splicing leads to proteins of altered function have been reported, including examples from stress-related genes (4, 11, 12). RNA sequencing studies have shown that plant alternative splicing is responsive to environmental stimuli including light (13, 14), cold (4, 15), and salt stress (9) as well as heat, drought, and pathogen treatments (16). Splicing factors are themselves subject to alternative splicing under

Significance

The ability of plants to acclimate and maintain productivity under changing environmental conditions is a topic of heightened concern because of climate change and increasing demands on agriculture. Plant stress acclimation involves multiple layers of gene regulation and posttranslational protein modifications. Pre-mRNA splicing patterns are greatly altered by stress, yet little is known about how stress signaling impinges upon the splicing machinery to mediate such changes. We found that one of the key stress signaling protein phosphatases can interact with and dephosphorylate a newly identified splicing regulator. This splicing regulator promotes growth during moderate-severity drought stress and mediates a dramatic shift toward increased splicing efficiency of stress and signaling-related genes which are prone to intron retention.

stress (17, 18), are extensively phosphorylated (19), and can affect stress responses (1, 20). While these and other studies have shown that abiotic stress alters pre-mRNA splicing, the mechanisms by which stress signaling communicates with the splicing machinery to control alternative splicing are not understood (3).

The Clade A protein phosphatase 2Cs (PP2Cs) have a prominent role in ABA and stress signaling via their interaction with the PYR/PYL/RCAR ABA receptors and regulation of SnRK2 kinase activity (21, 22). Among Clade A PP2Cs, the 3 HAI PP2Cs (HAI1, HAI2/AKP-Interacting protein1, and HAI3) are strongly induced by low ψ_w and have prominent effect on abiotic stress-associated phenotypes such as proline accumulation, growth regulation, and osmotic adjustment (23, 24). HAI1 is predominantly localized in the nucleus (24, 25). Phosphoproteomic analysis of *hai1-2* identified nuclear-localized proteins, including Serine-Arginine rich (SR) splicing factors (RSZ22, RSP31, and SCL30) as well RNA binding and RNA cap-binding proteins, as putative targets of HAI1 regulation (23). This finding was consistent with reports that splicing factor phosphorylation is responsive to a number of stress and hormone signals (17, 19, 26–29).

In parallel with our phosphoproteomic analysis of *hai1-2* (23), we conducted a yeast 2-hybrid screen for HAI1-interacting proteins. Subsequent analysis of one of these HAI1 interacting proteins found that it promotes growth during drought stress, influences splicing at intron retention sites, and binds to an RNA motif found adjacent to those introns. The RNA-binding activity of this protein was unexpected as it does not have a known RNA binding domain. These data identify a plant RNA-binding splicing regulator, show a specific effect of drought acclimation to promote splicing efficiency of IR-prone introns, and indicate a mechanism by which stress signaling can influence pre-mRNA splicing.

Results

HAI1-Interactor1 (HIN1) Is a Protein of Unknown Function Which Interacts with and Is Dephosphorylated by HAI1. HAI1 was used to screen a yeast 2-hybrid library prepared from seedlings acclimated to low ψ_w (30). Of the few strongly interacting proteins identified, the majority were Heat Shock (HSP) proteins and Ribosomal proteins, while 2 others were proteins of unknown function (*SI Appendix*, Fig. S1 *A* and *B*). Further study focused
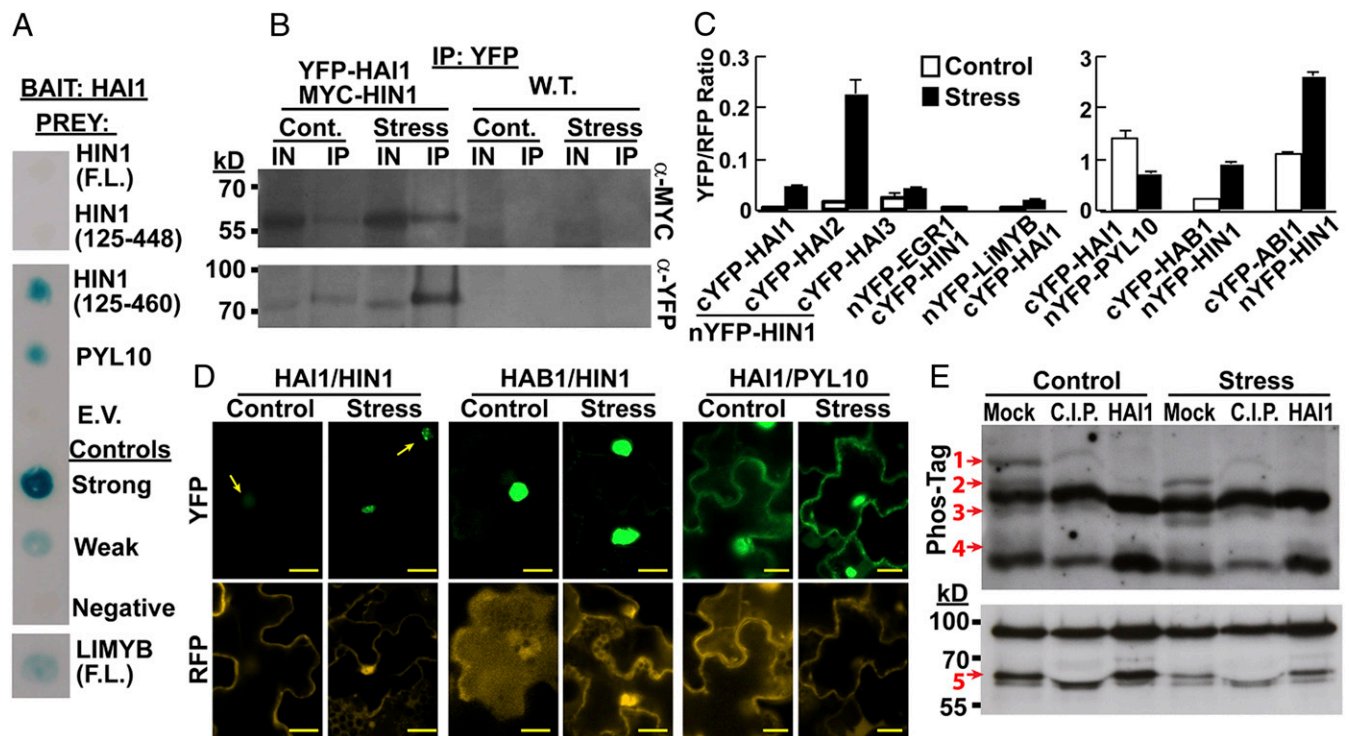

Fig. 1. HIN1 interacts with HAI1 as well as other Clade A PP2Cs and can be dephosphorylated by HAI1. (*A*) HAI1–HIN1 and HAI1–LIMYB interaction in yeast 2-hybrid assays. Colony lifts after β-galactosidase staining are shown. Strong, weak, and negative control interaction pairs provided with the ProQuest yeast 2-hybrid system were included for comparison. PYL10 was included as a positive control for HAI1 interaction. All interaction pairs showed consistent results in repeated assays. F.L., full length; E.V., empty vector. (*B*) Coimmunoprecipitation of YFP-tagged HAI1 and MYC-tagged HIN1. Both constructs were transiently expressed in Avr-PTO expressing *Arabidopsis* seedlings and immunoprecipitation performed 48 h after transfer of seedlings to fresh control plates (Cont.) or stress (−1.2 MPa) plates. Co-IP assays were also done with YFP-tagged EGR1 (a Clade E PP2C) as a negative control (*SI Appendix*, Fig. S1D), and both sets of assays included mock IP assays with untransformed Avr-PTO seedlings as a further negative control. IN, input; IP, immunoprecipitated sample. Results shown are representative of several replicate experiments. (*C*) Ratiometric BiFC quantification of relative interaction intensity (ratio of YFP fluorescence to that of the RFP reporter contained in the same vector). Experiments were performed by transient expression in Avr-PTO seedlings. After infiltration, seedlings were transferred to fresh control plates or to −1.2-MPa plates for 48 h before YFP and RFP fluorescence was quantified in individual cells. Data are means ± SE, *n* = 20 combined from 2 to 3 independent experiments. (*D*) Representative images of rBiFC assays reported in *C*. In all cases, interaction was observed in the nucleus. Arrows in the HAI/HIN1 YFP images show example of nuclei having faint HAI1–HIN1 interaction in the unstressed control or example of nuclei where the HAI1–HIN1 interaction was observed as nuclear speckles. Representative images of other interaction pairs are shown in *SI Appendix*, Fig. S2. (Scale bars, 20 μm.) (*E*) In vitro dephosphorylation assays. YFP-HIN1 immunoprecipitated from *35S:YFP-HIN1* plants in control and stress (−0.7 MPa, 96 h) treatments was dephosphorylated using Calf Intestinal Phosphatase (C.I.P.) or recombinant HAI1 (5 μg). Aliquots of the same samples were run on Phos-tag gel (*Top*) and SDS/PAGE (*Bottom*). Both blots were probed with antisera recognizing YFP. Red numbers along the left of the blots indicate phosphorylated forms of HIN1. The expected molecular weight of YFP-HIN1 is 81 kDa. The experiment was repeated with consistent results.

on AT3G11290, which we named HAI1-Interactor 1 (HIN1). The original HIN1 clone isolated was an N-terminal truncation (amino acids 125 to 460), and this interaction was confirmed by retransformation in the yeast 2-hybrid system (Fig. 1*A*). Truncating the C terminus (HIN1 125 to 448) abolished the interaction, indicating that HAI1 interacted with the C-terminal portion of HIN1 (Fig. 1*A*). HAI1 interaction with full-length HIN1 was not detected in yeast 2-hybrid assays, possibly because nuclei acid binding activity of the N-terminal domain interfered with the assay.

Coimmunoprecipitation confirmed HAI1–HIN1 interaction in planta and indicated that there was more extensive interaction in stress-treated plants (Fig. 1*B*). Ratiometric BiFC (rBiFC) (31) assays also indicated increased HAI1–HIN1 interaction during low ψ_w stress (Fig. 1*C*). HAI1–HIN1 interaction was detected in the nucleus, consistent with the predominant nuclear localization of HAI1 (24, 25). HIN1 also interacted with HAI2 and HAI3 as well as the Clade A PP2Cs HAB1 and ABI1 (Fig. 1 *C* and *D*). The HAB1 and ABI1 interactions had a more intense rBiFC signal; however, this was likely due to higher expression of these proteins in the rBiFC assays (*SI Appendix*, Fig. S1*C*) and does not necessarily indicate a greater interaction affinity. Interestingly, HIN1 interaction with HAI1, HAI2, or HAI3, but not the HAB1 or ABI1 interaction, was sometimes observed as speckles within the nucleus (Fig. 1*D* and *SI Appendix*, Fig. S2*A*). HIN1 had no detectable interaction with the Clade E PP2C EGR1 (32), which was used as a negative control for Co-IP (*SI Appendix*, Fig. S1*D*) and rBiFC (Fig. 1*C* and *SI Appendix*, Fig. S2*A*). The HAI1-PYL10 interaction was used as a positive control (Fig. 1 *A*, *C*, and *D*). Together these data demonstrated that HIN1 interacted with HAI1 and other Clade A PP2Cs. Note that HAI1 was tagged at the N terminus as this arrangement was previously

shown to be functional and correctly localized, while HAI1 with C-terminal tag was not (24).

HIN1 has 2 annotated MYB/SANT domains in its N terminus, while the C-terminal domain has no known function (*SI Appendix*, Fig. S3*A*). Blast search of *Arabidopsis* found that the closest HIN1 homolog is *LIMYB* (*At5g05800*; *SI Appendix*, Fig. S3*B*), which may be involved in expression of ribosomal genes (33). LIMYB had a weak, barely detectable interaction with HAI1 in both yeast 2-hybrid (Fig. 1*A*) and rBiFC (Fig. 1*C*) assays. *HIN1* and *LIMYB* were expressed at similar levels, and neither one was induced by low ψ_w (*SI Appendix*, Fig. S3*C*). Two other *HIN1*-related genes did not have detectable expression. To characterize HIN1 localization and dephosphorylation, we generated transgenic lines with expression of untagged HIN1 (*35S:HIN1*) or YFP-tagged HIN1 (*35S:YFP-HIN*; *SI Appendix*, Fig. S3*D*). The YFP-HIN1 fusion protein accumulated to the same level in control and stress treated plants (*SI Appendix*, Fig. S1*E*). DAPI staining confirmed YFP-HIN1 nuclear localization (*SI Appendix*, Fig. S3*F*). Note that transgenic lines with C-terminal HIN1-YFP fusion failed to accumulate detectable levels of the fusion protein.

Search of the PhosPhAT database (34) found experimentally validated HIN1 phosphorylation at S357 and S389 (35) and predicted phosphorylation at several additional sites (*SI Appendix*, Fig. S4). To determine whether HAI1 could dephosphorylate HIN1, YFP-HIN1 was immunoprecipitated, incubated with recombinant HAI1 or nonspecific phosphatase (C.I.P.), and analyzed on Phos-Tag gels. Both full-length YFP-HIN1 and a truncated form were detected after immunoprecipitation (Fig. 1*E*). HAI1 was even more effective than C.I.P. in dephosphorylation of full-length YFP-HIN1, as evidenced by loss of bands 1 and 2 on Phos-Tag gel (Fig. 1*E*). In contrast, HAI1 could not fully dephosphorylate the N-terminal
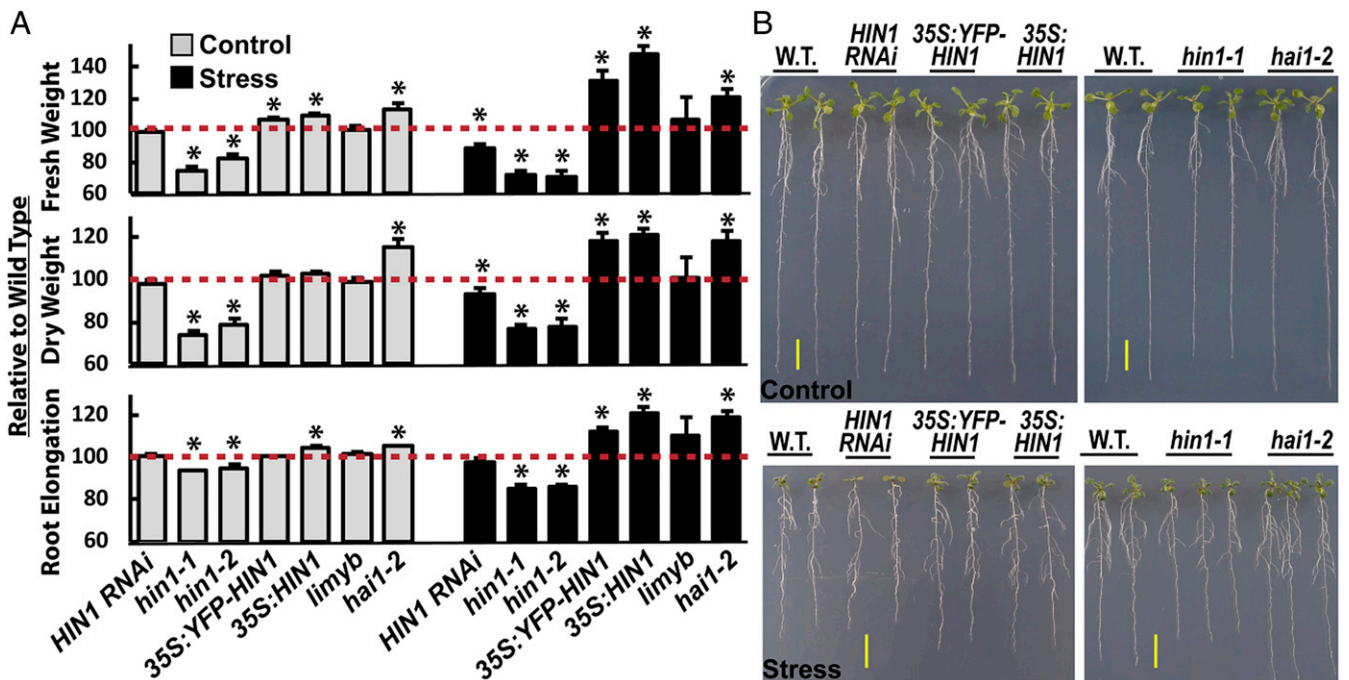

Fig. 2. HIN1 promotes growth during low ψ_w stress. (*A*) Seedling fresh weight, dry weight, and root elongation under unstressed control (−0.25 MPa) or stress (−0.7 MPa) conditions. The data for *35S:HIN1* and *35S:YFP-HIN1* are combined from 2 independent transgenic lines for each construct (*SI Appendix*, Fig. S3*D*). The HIN1 RNAi data are combined from 4 transgenic lines (*SI Appendix*, Fig. S3*E*). For growth assays, 5-d-old seedlings were either transferred to fresh control plates and allowed to grow for 5 d before data collection or transferred to low ψ_w stress plates (−0.7 MPa) and allowed to grow for 8 d before data collection. Data are means ± SE, *n* = 20 to 60 combined from 3 or 4 independent experiments. Asterisks indicate significant differences compared to WT (*P* ≤ 0.05 by 1-sample *t* test). WT growth data used for normalization are shown in *SI Appendix*, Fig. S6*B*. (*B*) Representative images of seedlings of each genotype at the time of data collection for both control and stress (−0.7 MPa) treatments. Representative images of *limyb* seedlings can be seen in *SI Appendix*, Fig. S6*C*. (Scale bars, 1 cm.)

HIN1 truncation (bands 3 and 4 on Phostag gel and band 5 on SDS/PAGE; Fig. 1E). Together with the yeast 2-hybrid data, these results indicated that HAI1 interacted with and dephosphorylated the C-terminal region of HIN1, either at the experimentally identified S357 and S389 sites or at other yet to be identified sites.

Phosphorylation can affect many aspects of protein function, including stability. Detection of YFP-HIN1 in the wild-type (WT) or *hai1-2* mutant background (where HIN1 may be more phosphorylated), after MG132 treatment found no evidence for decreased protein stability and in fact HIN1 accumulated to slightly higher level in the *hai1-2* background even before MG132 treatment (*SI Appendix*, Fig. S2B). This suggested that phosphorylation is unlikely to target HIN1 for degradation but may instead affect other aspects of HIN1 function.

HIN1 Promotes Growth Maintenance During Drought. We then tested whether HIN1 ectopic expression or loss of function affected low ψ_w response at the physiological level. As no *HIN1* T-DNA mutant was available, we first generated *HIN1* RNAi suppression lines. Later, we used Crispr/CAS9 editing to generate

loss of function mutants, *hin1-1* and *hin1-2*, both of which have frame-shift deletions near the HIN1 start codon (*SI Appendix*, Fig. S5). These mutants had significantly reduced growth compared to WT in both the unstressed control and under low ψ_w stress (Fig. 2 A and B). Five-day-old *hin1-1* and *hin1-2* seedlings were also smaller than WT at the time of transfer to the stress or control treatments (*SI Appendix*, Fig. S6A). *HIN1* RNAi lines had partial knockdown of *HIN1* expression (*SI Appendix*, Fig. S3E) and thus maintained normal growth in the unstressed control (Fig. 2 A and B). *HIN1* RNAi lines did, however, have decreased growth at low ψ_w, indicating that normal HIN1 expression was required for low ψ_w response. Conversely, transgenic lines with ectopic *HIN1* expression had enhanced growth maintenance during low ψ_w stress and slightly increased growth in the unstressed control (Fig. 2 A and B). In contrast with the HIN1 results, an *limyb* mutant had no significant effect on growth (Fig. 2A and *SI Appendix*, Figs. S3G and S6C), indicating that LIMYB and HIN1 have distinct functions. The growth phenotype of *hin1-1* and *hin1-2* was opposite to that of *hai1-2*, which had increased growth (Fig. 2), consistent
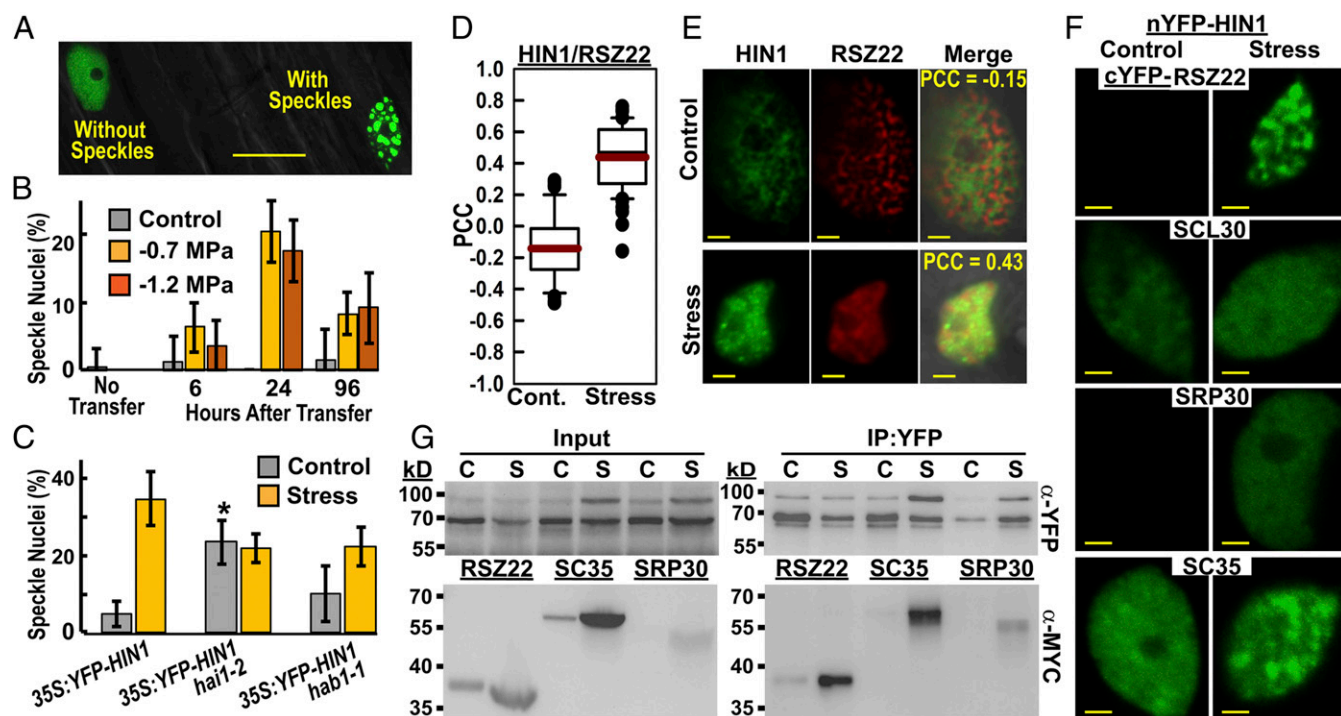

Fig. 3. Stress-induced HIN1 nuclear speckles and colocalization of HIN1 with pre-mRNA splicing factors. (A) Image of root cells of low ψ_w stress-treated (−0.7 MPa, 24 h) *35S:YFP-HIN1* with example of nuclei having diffuse nucleoplasmic localization or nuclear speckle-like localization of YFP-HIN1. (Scale bar, 20 µm.) (B) The frequency of nuclei (from root cells) having speckle-like pattern of YFP-HIN1 quantified after transfer of 5-d-old seedlings to either fresh control plates or PEG-infused agar plates of moderate severity (−0.7 MPa) or more severe (−1.2 MPa) low ψ_w stress. A control set of seedlings not transferred to new plate was also included. Nuclei were counted as speckled if 3 or more distinct foci of YFP-HIN1 were visible. Data are combined from 2 independent experiments with 150 to 350 nuclei counted for each treatment. Error bars indicated the 95% confidence interval. (C) Frequency of nuclei with speckle-like YFP-HIN1 localization for plants expressing *35S:YFP-HIN1* in the WT, *hai1-2*, or *hab1-1* backgrounds. Four independent experiments were conducted with 50 to 70 nuclei counted for each genotype in each experiment. Data shown are means ± SE (*n* = 3 to 4). Asterisk indicates a significant difference compared to WT in the same treatment (*P* ≤ 0.05 by *t* test). (D) YFP-HIN1 and RSZ22-RFP colocalization quantified by Pearson correlation coefficient (PCC). The proteins were transiently expressed in *Arabidopsis* seedlings under control or low ψ_w stress (−0.7 MPa, 24 h) conditions. Red lines indicate the mean; box and whiskers indicated the 25th to 75th and 5th to 95th percentiles, respectively; and black circles show outlying data points. PCC differed significantly between control and stress (*P* ≤ 0.05, *t* test, *n* = 57 to 62 for each treatment). Analysis of HIN1 colocalization with additional splicing factors can be found in *SI Appendix*, Fig. S7. (E) Representative images of HIN1-RSZ22 nuclear colocalization in stress and control treatments. The PCC value for the colocalization for each image is indicated. Representative images of HIN1 colocalization with additional splicing factors can be found in *SI Appendix*, Fig. S7. (Scale bars, 2 µm.) (F) BiFC assays of HIN1 interaction with splicing factors. After infiltration, seedlings were transferred to fresh control plates or to −0.7 MPa plates for 48 h before imaging. Additional BiFC assays using BiFC tag attached to the RSZ22 N terminus are shown in *SI Appendix*, Fig. S8A. (Scale bars, 2 µm.) (G) Coimmunoprecipitation of YFP-HIN1 and MYC-tagged splicing factors. Both constructs were transiently expressed in Avr-PTO *Arabidopsis* seedlings and immunoprecipitation performed 48 h after transfer of seedlings to fresh control plates (Cont.) or stress (−0.7 MPa) plates. IP, immunoprecipitated sample; C, control; S, stress. The experiment was repeated with essentially identical results.

with previous results from our laboratory (23). Note that the moderate-severity −0.7-MPa stress treatment used in these experiments reduced, but did not completely inhibit, growth of WT (*SI Appendix*, Fig. S6B) and did not affect plant survival for any of the genotypes.

Nuclear Speckle Localization as Well as Colocalization and Interaction with Splicing Factors Indicate HIN1 Function in Pre-mRNA Splicing. YFP-HIN1 was typically diffusely localized in the nucleoplasm; however, nuclei of stress-treated plants sometimes had a speckle-like pattern (Fig. 3A). Counting of nuclei with diffuse versus speckle-like pattern (defined as nuclei having 3 or more clearly visible speckles) showed that low ψ_w significantly increased the frequency of speckle-like HIN1 localization (Fig. 3B). When YFP-HIN1 was expressed in the *hai1-2* background, frequency of the speckle-like localization in unstressed plants increased significantly (Fig. 3C), indicating that HIN1 localization was influenced by HAI1. Interestingly, *hab1-1* had lesser effect on HIN1 localization (Fig. 3C).

Nuclear speckle localization is often observed for proteins associated with pre-mRNA splicing (36). Consistent with this idea, we found that HIN1 colocalized and interacted with several splicing factors. The serine-arginine rich splicing regulator RSZ22 had stress-induced colocalization with HIN1 (Fig. 3 D and E). This was particularly interesting as RSZ22 was also identified as a putative dephosphorylation target of HAI1 by phosphoproteomic analysis (23). HIN1 had limited or no colocalization with other splicing factors identified as putative HAI1 targets (RSZ33, RSP31, and SCL30; *SI Appendix*, Fig. S7A) but did partially colocalize with SC35, SRP30, and SRP34 (*SI Appendix*, Fig. S7B).

BiFC assays detected HIN1 interaction with RSZ22, SCL30, SRP30, and SC35 (Fig. 3F and *SI Appendix*, Fig. S8A). The RSZ22 and SRP30 interactions were only detected under low ψ_w stress. Interaction of RSZ22, SC35, and SRP30 with HIN1 during low ψ_w stress was confirmed by coimmunoprecipitation (Fig. 3G). Interestingly, BiFC assays using HAI1 found that the phosphatase may interact with RSZ22, SCL30, and SC35 (*SI Appendix*, Fig. S8), albeit that the intensity of BiFC signal was less than for the splicing factor–HIN1 interactions and only observed under stress. BiFC of HAI1 with SRP30 may also have generated a weak signal under stress but was inconclusive. Together, these data demonstrated that HIN1 (and HAI1) interacted with several known splicing factors and raised the possibility that HIN1 and HAI1 have roles in pre-mRNA splicing during low ψ_w stress.

Drought Acclimation Increases Splicing Efficiency at Intron Retention Sites. RNA sequencing was used to explore gene expression and alternative splicing in WT and *35S:HIN1* after acclimation to moderate-severity low ψ_w stress (−0.7 MPa, 96 h) where *35S:HIN1* had enhanced growth maintenance. WT had 2,855 differentially expressed genes (DEGs) in response to stress treatment (fold change ≥ 1.5, adjusted $P \leq 0.05$; *SI Appendix*, Fig. S9A and Dataset S1). Unstressed *35S:HIN1* had 422 DEGs compared to unstressed WT, while stress-treated *35S:HIN1* had 315 DEGs relative to stress-treated WT (*SI Appendix*, Fig. S9A and Datasets S2 and S3). The stress-regulated DEGs in WT were enriched for abiotic stress-related Gene Ontology (GO) terms; however, DEGs affected by *35S:HIN1* were not enriched for stress-related GO terms (Dataset S4), and there was little overlap of DEGs between *35S:HIN1*
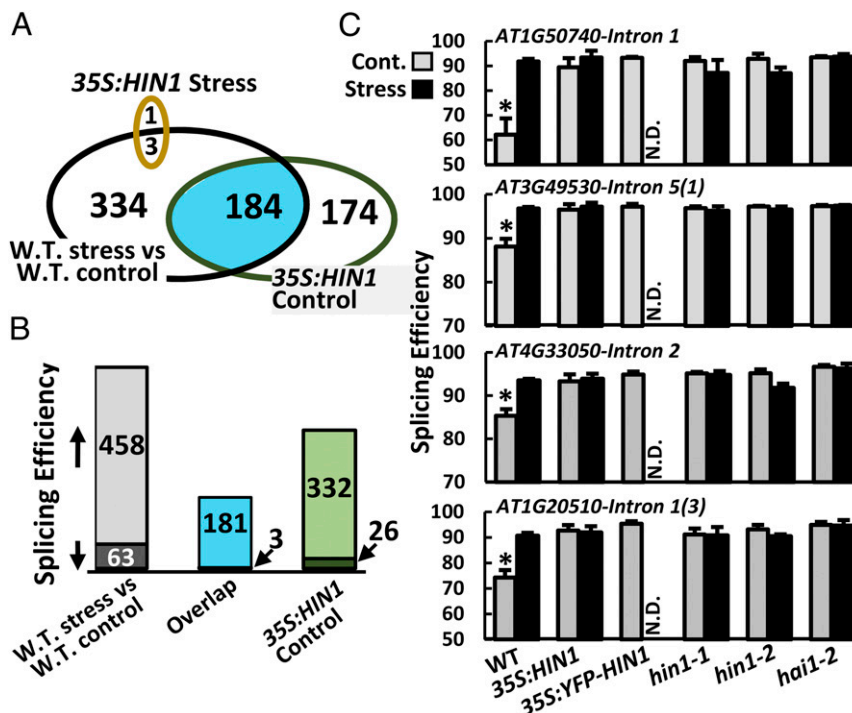

Fig. 4. Low ψ_w or expression of *35S:HIN1* in unstressed plants increases splicing efficiency of an overlapping set of IR-prone introns. (A) Comparison of introns with significantly altered (Q ≤ 0.05) IR under stress (−0.7 MPa, 96 h) in WT (Dataset S5) versus introns with significantly altered IR in *35S:HIN1* under either control or stress treatments (Datasets S8 and S10). (B) Number of introns with increased and decreased splicing efficiency for WT stress compared to control, *35S:HIN1* control compared to WT control, and the overlapping introns between the 2 sets. (C) QPCR assay of splicing efficiency of the indicated introns. Note that AT3G49530 and AT1G20510 are encoded on the reverse genomic strand. Therefore, the affected intron is number 5 or 3 when counting from 5′ to 3′, respectively, on the forward genomic strand, as listed in the Datasets S5–S15, but is intron 1 in the actual transcript. Data are means ± SE (*n* = 3 to 10). Asterisks indicate that the WT control was significantly different from all other genotypes and treatments (P ≤ 0.05, *t* test). RNAseq read depths for these genes as well as diagram of primer positions used for the splicing assays can be found in *SI Appendix*, Fig. S11A. QPCR assay of total mRNA level for these genes can be found *SI Appendix*, Fig. S11B. Note that *35S:YFP-HIN1* was not assayed in the stress treatment (N.D., not determined).

and WT (*SI Appendix*, Fig. S9A). These data suggested that HIN1 was not a major effector of stress-regulated gene expression.

The effect of low ψ_w acclimation on pre-mRNA splicing patterns was examined using an established workflow to identify splice variants that had a stress-induced change in abundance which could not be accounted for by change in total transcript level (37, 38). Among the splicing events significantly (Q < 0.05) affected by low ψ_w in WT, IR was most prevalent (521 sites from 400 genes; Fig. 4A and Dataset S5), while ES was the least prevalent (70 sites from 69 genes; Dataset S6). There was an intermediate number of transcripts with altered donor/acceptor site usage (126 sites from 113 genes; Dataset S7). Interestingly, among the stress-affected IR sites there was a striking shift (88%) toward increased splicing efficiency (reduced IR) at low ψ_w (Fig. 4B and Dataset S5). In contrast, among the ES events, there were an equal number of sites with low ψ_w promotion of ES versus those with low ψ_w repression of ES (Dataset S6). These data suggested that there may be a low ψ_w-regulated mechanism(s) to increase splicing efficiency of specific introns that are otherwise prone to IR. It was also interesting to note that there was limited overlap between the genes with altered splicing at low ψ_w versus DEGs at low ψ_w (*SI Appendix*, Fig. S9B), consistent with previous reports of little overlap of stress-regulated DEGs and genes with stress-affected alternative splicing (9, 15, 16).

Ectopic HIN1 Expression in Unstressed Plants Mimicked the Effect of Low ψ_w Acclimation to Increase Splicing Efficiency of Specific Introns.
In the unstressed control, *35S:HIN1* significantly (Q < 0.05) altered IR at 358 introns from 255 genes (Fig. 4A and Dataset S8). Here again, it was striking that 93% of the sites where IR was affected by *35S:HIN1* had increased splicing efficiency (Fig. 4B). More than half the IR sites affected by *35S:HIN1* in the unstressed control were also affected by low ψ_w stress in WT (Fig. 4A and Dataset S9; overlap between the 2 datasets was significantly more than random; Fisher's exact test, $P = 2.7 \times 10^{-231}$). In this overlapping set of introns the shift toward increased splicing efficiency was even more dramatic (98%; Fig. 4B and Dataset S9). These data demonstrated that ectopic expression of HIN1 was sufficient to duplicate the effect of low ψ_w for more than one-third of the introns where low ψ_w-induced increase of splicing efficiency was observed.

The genes containing these introns where splicing efficiency was enhanced by low ψ_w acclimation and by *35S:HIN1* were enriched for abiotic stress-related GO terms and also enriched for calcium binding proteins (Dataset S13). It was also interesting to note that classification of introns affected by stress and *35S:HIN1* based on position in the pre-mRNA (first intron from the 5′ end, last intron at the 3′ end, middle intron, or only intron), found significant overrepresentation of last introns compared to first introns (4- to 5-fold more last introns; *SI Appendix*, Fig. S10). While the exact meaning of this unequal intron distribution is unclear, it indicates that the effect of HIN1 on splicing is distinct from that of the 5′ cap binding complex, which preferentially affects splicing at first introns (39). The bias toward last introns is partially similar to the effect mutating SDG725 (a rice histone H3 lysine 6 methyltransferase) which decreased IR in the 3′ region of pre-mRNAs but increased it in the 5′ region (40). The mechanism by which change in histone methylation could have such a position-specific effect on splicing is also unclear.

The effect of stress, *35S:HIN1*, *hin1* mutants, and *hai1-2* on IR of 4 selected genes was validated by QPCR using intron primers and primers spanning exon–intron junctions (primer positions and RNAseq read depths for the sites assayed are shown in *SI Appendix*, Fig. S11A). In these assays, *35S:HIN1* and *35S:YFP-HIN1* had increased splicing efficiency in the unstressed control, consistent with the RNAseq results. Interestingly, *hin1-1* and *hin1-2* also had high splicing efficiency in the unstressed control (Fig. 4C). These results suggest that HIN1 may act as a splicing
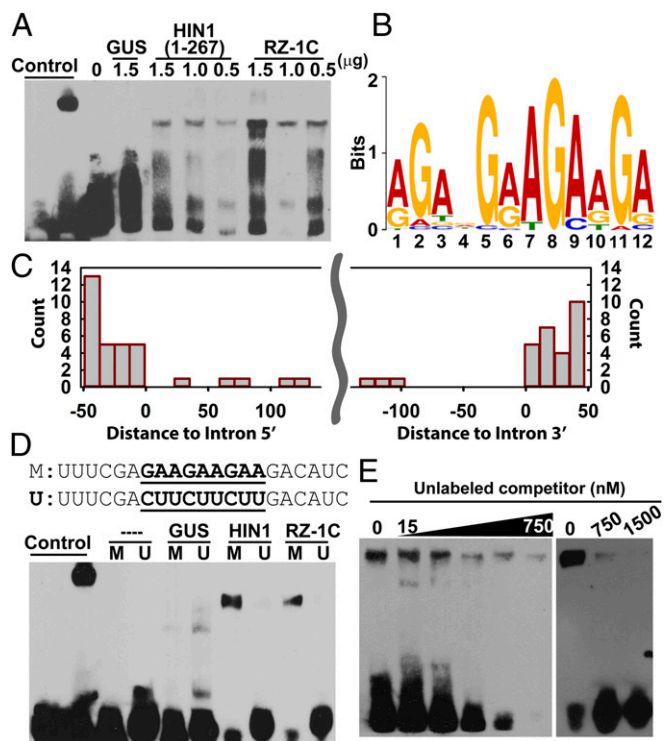

Fig. 5. HIN1 is an RNA binding protein that recognizes an Exon Splicing Enhancer (ESE)-like GAA cis-element. (*A*) RNA EMSA assay using the N-terminal half of HIN1 (amino acids 1 to 267) and full-length RZ-1C with total RNA isolated from WT seedlings. RZ-1C is a previously characterized RNA binding protein which was used as a positive control. β-glucouronidase (GUS) protein expressed in *Escherichia coli* was used as a negative control. Each lane contained the indicated amount of protein and 12.5 ng of total RNA extracted from WT seedlings. The control lanes contain control RNA and RNA binding protein supplied with the assay kit (*Methods*). The experiment was repeated with consistent results. (*B*) Enriched motif found associated with the 181 introns whose splicing efficiency was increased in stress treated WT or unstressed *35S:HIN1* (Fig. 4B). The sequence of each intron plus 50 bases of flanking exon sequence on each side was used for MEME search for enriched motifs. The motif shown was the most strongly enriched and had an E value of 1.2e-004 in the MEME analysis. (*C*) Locations of the motif shown in *B* relative to intron 5′ or 3′ ends. For each occurrence of the motif (Dataset S14) it was determined which end of the intron it was closer to, and then the distance to that end of the intron was calculated and histogram of those distances was plotted. Wavy line in the middle of the graph indicates that there is a variable amount of intron sequence between the 5′ and 3′ intron–exon junctions. (*D*) RNA EMSA assay of N-terminal HIN1 and RZ-1C binding to the motif shown in *B*. Control lanes are the same as in *A*. Samples incubated without protein or with GUS were used as negative controls. M is the specific motif and surrounding sequence as found in intron 1 of At1g50740 (Datasets S13 and S15). U indicates RNA probe where the core 9-bp GAA repeat has been changed to CUU. Each lane contained 7.5 nM of the labeled RNA probe and 1.5 μg of the indicated protein. The experiment was repeated with consistent results. (*E*) Competition assay using N-terminal HIN1 and the specific probe shown in *B* (7.5 nM) along with increasing concentrations of unlabeled competitor probe. In each lane, 1.5 μg of HIN1 was used.

inhibitor with *35S:HIN1* and *35S:YFP-HIN1* having a dominant negative effect. Also, *hai1-2* had increased splicing efficiency in the unstressed control (Fig. 4C). Both the enhanced splicing efficiency in unstressed *hai1-2* and enhanced growth maintenance of *hai1-2* under low ψ_w stress (Fig. 2) were similar to *35S:HIN1* and consistent with increased level of YFP-HIN1 protein accumulation in the *hai1-2* background compared to WT (*SI Appendix*, Fig. S2B). QPCR assays confirmed that total transcript level of these genes was not substantially altered by low ψ_w or in the mutant or transgenic lines (*SI Appendix*, Fig. S11B).

The amount of IR transcript that accumulates can be influenced by both the frequency of IR and stability of the IR transcript relative to the fully spliced transcript. RNA stability assays (Cordycepin treatment) found that the IR transcripts of *AT3G49530*, *AT4G33050*, and *AT1G20510* were less stable than the fully spliced transcripts. This indicated that the levels of IR versus fully spliced transcript shown in Fig. 4*C* may underestimate the amount of IR that occurs. The *35S:HIN1* plants did not differ from WT in the stability of these fully spliced or IR transcripts. Stability of *AT1G50740* IR transcript was relatively high (*SI Appendix*, Fig. S12), consistent with the high level of *AT1G50740* IR transcript observed in unstressed WT (Fig. 4*C*). This latter observation also seems consistent with reports that not all IR transcripts are efficiently targeted for nonsense-mediated decay (NMD) even when they have the typical NMD hallmarks such as a premature termination codon with a short ORF and long 3′ UTR (8, 41). Together these observations indicate that many of the IR transcripts affected by stress and *35S:HIN1* may be rapidly degraded and thus reduce the amount of protein translated. However, a portion of the IR transcripts may be relatively stable and, as many of them are affected in last or middle introns, will produce truncated or altered protein isoforms.

Over our whole RNAseq dataset, there was little overlap between genes where *35S:HIN1* affected IR versus DEGs in WT or *35S:HIN1* (*SI Appendix*, Fig. S9 *C–E*), again indicating that the effect of stress and *35S:HIN1* on IR was distinct from regulation of total transcript levels. The *35S:HIN1* had little additional effect on IR at low ψ_w (Fig. 4*A* and Dataset S10). Also, *35S:HIN1* had little effect on ES (only 12 and 22 exons significantly affected under stress or control conditions, respectively; *SI Appendix*, Fig. S9*F* and Dataset S11) and almost no effect on donor/acceptor site usage (only 17 sites significantly affected; *SI Appendix*, Fig. S9*G* and Dataset S12). Thus, regulation of IR was the most prominent, and perhaps the most direct, effect of HIN1.

HIN1 Binds to an ESE-Like Motif Enriched at IR Sites Where Low ψ_w and HIN1 Enhance Splicing Efficiency. The effect of HIN1 on IR raised the question of whether HIN1 is an RNA binding protein. We found that the N-terminal portion of HIN1 (amino acids 1 to 267) could bind plant total RNA in RNA-EMSA assay (Fig. 5*A*). The extent of HIN1 RNA binding was similar to that of RZ-1C which was used as a positive control. RZ-1C contains an RNA Recognition Motif and is required for efficient splicing of genes involved in development and flowering regulation (42).

To identify a putative HIN1 binding motif, a MEME search was conducted using introns (entire intron plus 50 bases of 5′ and 3′ flanking exon sequence) that had increased splicing efficiency in WT at low ψ_w and in unstressed *35S:HIN1* (Dataset S9). The most significantly enriched motif was a 12-bp GA-rich sequence which was present in exon sequence flanking either the 5′ or 3′ end of introns but rarely found inside introns (Fig. 5 *B* and *C* and Dataset S14). To test the robustness of this result using an expanded search space, the MEME search was repeated using introns with increased splicing efficiency in WT at low ψ_w and in unstressed *35S:HIN1* at a $P \leq 0.001$ cutoff (Dataset S15). This expanded set of introns had the same characteristics of high overlap between low ψ_w-treated WT and *35S:HIN1*, extreme shift toward increased splicing efficiency (*SI Appendix*, Fig. S13 *A* and *B*), enrichment of abiotic stress-related GO terms (Dataset S13), and overrepresentation of last (3′) introns compared to first (5′) introns (*SI Appendix*, Fig. S10). This larger MEME search found a very similar GAA repeat motif present in flanking sequence around introns (*SI Appendix*, Fig. S13 *C* and *D* and Dataset S14). The GAA repeat and placement of motifs from both searches was similar to ESE sequences of metazoan genes (5–7) and similar to putative cis-elements associated with light regulated IR in *Physcomitrella patens* (13) as well as binding motifs of some plant SR-type splicing factors (43).

Both HIN1 and RZ-1C could bind a synthetic RNA probe containing the GAA repeat motif plus surrounding sequence based on sequence 47 bases upstream of the first intron of *At1g50740* (Fig. 5 *D* and *E*). In contrast, HIN1 (and RZ-1C) did not specifically bind probes where the core 9 base GAA repeat sequence was fully mutated (Fig. 5*D*) or reduced to GAAGA (*SI Appendix*, Fig. S13*E*). This indicated that at least 2 complete GAA repeats were required for HIN1 binding. Together these analyses demonstrated that HIN1 has sequence-specific binding to an ESE-like cis-element enriched around introns where stress and HIN1 promote splicing efficiency. The MEME search did not find this enriched motif around all stress- and HIN1-affected introns (Dataset S14). However, it should be noted that our analysis likely underestimates the frequency of this ESE-like sequence as some occurrences of this motif may lie in exon sequence just outside of the search window. It is also possible that the 2 or more GAA sequences required for HIN1 binding could be separated by intervening sequence or part of a specific type of RNA secondary structure. This may in turn be consistent with how the MYB/SANT domains in HIN1 N-terminal region, which presumably are the part of the HIN1 protein directly involved in RNA binding, are separated by intervening amino acid sequence enabling them to bind to physically separate GAA elements.

HIN1 Is a Plant-Specific Protein. The finding that HIN1 had sequence-specific RNA binding was surprising given that HIN1 has no annotated RNA binding domain. Rather, the N-terminal portion of HIN1 used in the RNA binding assays is annotated as having 2 MYB/SANT domains. MYB domains bind DNA while SANT domains are structurally related but have functionally diverged and are often present in chromatin associated proteins (44, 45). However, alignment of the HIN1 and LIMYB SANT domains with MYB/SANT domains of chromatin-associated or DNA-binding proteins from both plants and metazoans found that the HIN1 and LIMYB SANT domains are highly diverged from other MYB/SANT domains (*SI Appendix*, Fig. S14). Also, the placement of the HIN1 SANT domains in the N-terminal portion of the protein differs from many other SANT domain proteins. The only possible precedent we could find for SANT domain RNA binding was a large-scale proteomics screening for mammalian RNA-binding proteins which identified MSANTD2 and MSANTD3 (46). However, RNA binding of these proteins was not validated, and their MYB/SANT domains have only limited similarity to those of HIN1 (*SI Appendix*, Fig. S14). The GAA-containing RNA sequence that HIN1 binds to is similar to a GAAGAA sequence enriched in DNA sites associated with Histone 3 acetylation regulated by the *Arabidopsis* SANT-domain protein Powerdress (PWR) (45); however, the PWR SANT domain is also diverged from that of HIN1 (*SI Appendix*, Fig. S14).

Protein blast searches found HIN1 orthologs in dicots and monocots, although the monocot orthologs were not as strongly conserved. In contrast, no proteins with significant homology to HIN1 were found in lower plants, algae, or animals (Dataset S16). There was a weak relationship of HIN1 to short domains within fungal proteins of unknown function (Dataset S16). This analysis indicated that HIN1 is a plant-specific protein. Despite this lack of protein sequence similarity, analysis of HIN1 by the structural prediction platform I-Tasser (47) found limited structural similarity to spliceosome and RNA-binding proteins as well as components of the nuclear pore complex (*SI Appendix*, Fig. S15). Although not conclusive by itself, this was consistent with our demonstration of HIN1 RNA binding and its effect on IR.

Discussion

Three major conclusions from our study provide insight into how plant alternative splicing is regulated and how it impacts abiotic
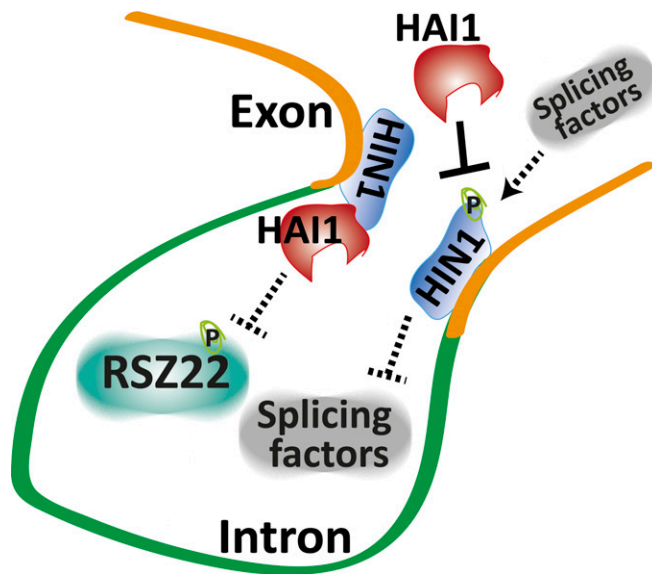
Fig. 6. Possible mechanisms of HAI1-HIN1 function in splicing regulation. Dephosphorylation of HIN1 by HAI1 (and other Clade A PP2Cs) may affect HIN1 interaction with other splicing-related proteins. HIN1 binding to exon regions near intron–exon junctions may also affect the recruitment or exclusion of other splicing factors, including those that bind to similar RNA cis-element sequences as HIN1. An alternative, and not mutually exclusive, hypothesis is that HIN1 recruits HAI (and perhaps other Clade A PP2Cs) to specific sites in order to facilitate dephosphorylation of other target proteins, such as RSZ22 and other splicing-related proteins identified by phosphoproteomic analysis of *hai1-2* (24). One or a combination of these mechanisms underlie the ability of HIN1 to affect splicing of specific IR-prone introns.

stress responses. First, our splicing analysis, RNA binding assays, and phylogenetic analysis show that HIN1 is a previously unknown and unexpected type of plant-specific RNA-binding protein and splicing regulator. Second, HIN1–HAI1 interaction, as well as HAI1 dephosphorylation of HIN1, provides a link between stress signaling and pre-mRNA splicing. Third, the shift toward increased splicing efficiency of IR-prone introns during acclimation to moderate-severity low ψ_w indicates a specific, and also unexpected, effect of drought acclimation on IR that has yet to be explored. The genes where low ψ_w and *35S:HIN1* led to enhanced splicing efficiency were enriched for abiotic stress and signaling-related functions. Together with the enhanced growth maintenance of *35S:HIN1* during low ψ_w, these results demonstrated that HIN1 and regulation of pre-mRNA splicing are important for drought acclimation.

The effect of HIN1 on IR and its binding to a GAA-containing motif enriched in intron-flanking regions indicated that HIN1 may be functionally similar to splicing enhancer and inhibitor proteins which have been best characterized in metazoans but are not fully understood in any organism. Although we cannot rule out other possibilities, our data suggest that HIN1 acts as a splicing inhibitor. HIN1 binding to ESE-like elements may act to recruit splicing-related proteins which interact with HIN1 and may also block RNA-binding of other splicing-associated proteins which associate with the same, or similar, RNA motif (Fig. 6). Several types of plant SR proteins, including the HIN1-colocalized and HIN1-interacting proteins RSZ22 SC35, SRP30, and SRP34, are thought to bind cis-elements that regulate splicing (18). RSZ22 has been shown to interact with components of the U1 SNRP and may recruit it to the 5′ splice site (18, 48). Interestingly, RSZ22 preferentially binds to a different RNA motif than HIN1 (49); perhaps these proteins colocalize and interact when bound to adjacent RNA sites or when one or both of them is not bound to

RNA. The SC35-related protein SCL30 (and perhaps SC35 itself) bound to a GAA-containing RNA motif enriched in sequences within 100 bases of SC35/SCL30-regulated introns (43). Also, a motif similar to the GAA-containing motif we identified was enriched in the intron-flanking regions of SR45-associated transcripts, including ABA and stress-related genes (20). SR45 mutant and overexpression lines had altered ABA sensitivity. Such results, along with the results presented here, hint at a complex interaction and competition between proteins that bind to GAA-containing ESE-like elements and indicate that such interaction/competition is important for abiotic stress and ABA responses (Fig. 6). Such interactions may explain why either loss of HIN1 function or ectopic HIN1 expression could lead to enhanced splicing efficiency in unstressed plants. It is possible that ectopic expression of HIN1 sequesters other splicing factors or that that higher levels of HIN1 expression lead to different posttranslational modification (such as phosphorylation) that determines HIN1 function. Such HIN1 interactions and regulation by posttranslational modification may also explain the more prominent localization of HIN1 in nuclear speckles during stress and could explain the observation that *35S:HIN1* had almost no additional effect on splicing during low ψ_w stress. Whether speckle-localized HIN1 is active or whether the speckles are sites where HIN1 is sequestered, as is thought to be the case for other splicing factors, is uncertain.

The increased prevalence of HIN1 nuclear speckles in the *hai1-2* background and decreased IR of HIN1-affected genes in *hai1-2* indicate that HAI1 affects HIN1 function. However, it is unlikely that this occurs via effects on HIN1 RNA binding since this occurred at the N-terminal region, while HAI1 interacted with and dephosphorylated the C-terminal portion of HIN1. Instead, HAI1 regulation of HIN1 phosphorylation could affect interaction with other splicing-related proteins. Another, not mutually exclusive, possibility is that recruitment by HIN1 brings HAI1 to the appropriate location to dephosphorylate splicing factors such as RSZ22 or others (Fig. 6). RSZ22 is known to be affected by phosphorylation as phosphatase and kinase inhibitors alter its mobility and distribution in nuclear speckles (50–52). More generally, splicing factor phosphorylation is known to be affected by abiotic stress (32, 53, 54), and our data indicate that HAI1–HIN1 interaction is part of a previously unknown mechanism connecting stress signaling to splicing factors.

Of the HIN1-related genes in *Arabidopsis*, only LIMYB has been characterized. LIMYB was reported to interact with Ribosomal Protein L10 and down-regulate expression of ribosomal protein genes leading to a general down-regulation of translation to defend against viral replication (33). They interpreted the function of LIMYB as that of a transcription factor and found enrichment of LIMYB on ribosomal gene promoters in chromatin immunoprecipitation assays. However, they did not test whether LIMYB directly bound DNA or was part of a larger protein complex associated with ribosomal genes, perhaps including proteins involved in cotranscriptional processing of ribosomal RNAs. Regardless of whether LIMYB is also an RNA binding protein, its function seems divergent from that of HIN1 as *limyb* did not affect growth, and LIMYB only weakly interacted with HAI1. Also, the 2 experimentally observed phosphorylation sites in the C-terminal domain of HIN1, which are likely targets of HAI1 dephosphorylation, are not conserved in LIMYB (*SI Appendix*, Fig. S4). It must also be noted that fresh weight and dry weight of *hin1* mutants was reduced by nearly one-fourth even in the unstressed control. Whether or not this reduced growth was caused solely by effects on splicing is unknown. While our data establish a role for HIN1 in splicing regulation, we do not rule out the possibility that HIN1 has additional functions which may affect the physiological phenotypes of *hin1* mutants or *35S:HIN1* plants.

Other studies of stress-induced changes in splicing patterns have not, to our knowledge, observed the shift toward increased splicing efficiency of IR-prone introns that we observed. In fact, it has been reported that short-term salt stress or heat stress increased the prevalence of IR (9, 55). A key difference between our study and others is that we exposed plants to a moderate-severity low ψ_w over 96 h to allow time for stress acclimation. Genes where HIN1 and low ψ_w led to enhanced splicing efficiency were enriched for stress and signaling-related GO terms. A number of these were *Early Response to Desiccation* (*ERD*) genes including *ERD6, 7, 10, 13*, and *14* (Datasets S9 and S15) as well as other genes known to be transcriptionally induced by stress or involved in stress signaling (for example, MAP Kinase 3 and many genes related to calcium signaling). Total transcript level of these genes was generally unchanged in our longer-term low ψ_w treatment or by *35S:HIN1*. For genes such as the ERDs, the implication is that these genes were transcriptionally regulated in the early acute phase of stress response, while splicing regulation of these genes is initiated later, or persists longer, during low ψ_w acclimation. In the unstressed control, a high level of IR leading to the production of unstable transcripts or transcripts that do not encode an active protein may be means to ensure that production of stress-associated proteins is turned off. Increased splicing efficiency during stress would amplify the transcriptional activation or extend the duration of increased protein production from these genes during drought acclimation.

Manual inspection of stress and *35S:HIN1*-affected transcripts found that nearly all of the IR transcripts had premature stop codons, consistent with other studies of plant alternative splicing (10). If the transcript is stable and transcribed, it is likely that the truncated protein produced is nonfunctional. However, in some cases, a protein of altered function may be produced. For example, IR of the last intron of NTL6/NAC062 (AT3G49530; Fig. 4*C*) produces a transcript encoding a truncated protein lacking the membrane tethering domain. This truncated protein would no longer need to be released from the plasma membrane by stress- or ABA-induced cleavage to enter the nucleus and regulate gene expression (56, 57). Interestingly, intron retention leading to a similar C-terminal truncation of an orthologous NAC transcription factor has been observed in maize (58), suggesting that alternative splicing may be a conserved mechanism to regulate NAC transcription factor function. The effect of HIN1 on growth at low ψ_w may represent a cumulative effect of altered function or altered abundance of signaling and stress-related proteins, such as NAC062, encoded by genes with HIN1-regulated changes in IR. Case-by-case characterization is

required to determine which of the IR transcripts we observed lead to decreased protein level and which lead to the production of functionally distinct isoforms. As stated above, we do not rule out the possibility that other aspects of HIN1 molecular function could also contribute to its physiological phenotypes.

Our data also show that HAI1 may interact with several splicing factors. This is consistent with phosphoproteomic analysis of *hai1-2* that identified putative HAI1 dephosphorylation targets related to splicing and RNA processing (23). Characterization of these additional HAI1-regulated proteins will be a promising approach to reveal further connections of stress signaling to pre-mRNA splicing. This could include regulation of IR events and splice donor–acceptor site changes affected by stress but not affected by HIN1. This in turn will lead to better overall understanding of how and why abiotic stress has such a pronounced effect on alternative splicing, a question which continues to become more prominent in plant stress biology.

Methods

Yeast 2-hybrid screening was conducted using the ProQuest yeast 2-hybrid system (Life Technologies) using full-length HAI1 as bait and a library prepared from low ψ_w-acclimated *Arabidopsis* seedlings. Low ψ_w treatments were performed using polyethylene glycol-infused agar plates (23, 32). Splicing factors for colocalization and interaction experiments were subcloned from previously reported clones (36) or amplified from *Arabidopsis* cDNA. RNA sequencing of *35S:HIN1* was performed in the same set of experiments as our previously presented analysis of *ahl10-1* (23) and used the same WT controls. Thus, WT stress versus control gene expression analysis presented in Dataset S1 is the same as that presented in datasets S6 and S7 of Wong et al. (23) and is presented again here for clarity. Detection of alternative splicing events affected by low ψ_w stress or *35S:HIN1* followed established methods (13, 59). Further description of all methods including construction of RNAi lines, use of Crispr/CAS9 editing to generate HIN1 mutants, protein interaction assays, and statistical methods can be found in SI Appendix, Supplemental Methods. RNA sequencing data can be accessed in the Gene Expression Omnibus (GEO) repository with accession number GSE127805 at https://www.ncbi.nlm.nih.gov/geo/query/acc.cgi?acc=GSE127805.

1. S. Filichkin, H. D. Priest, M. Megraw, T. C. Mockler, Alternative splicing in plants: Directing traffic at the crossroads of adaptation and environmental stress. *Curr. Opin. Plant Biol.* **24**, 125–135 (2015).
2. T. Laloum, G. Martín, P. Duque, Alternative splicing control of abiotic stress responses. *Trends Plant Sci.* **23**, 140–150 (2018).
3. A. S. N. Reddy, Y. Marquez, M. Kalyna, A. Barta, Complexity of the alternative splicing landscape in plants. *Plant Cell* **25**, 3657–3683 (2013).
4. R. Huertas *et al.*, Arabidopsis SME1 regulates plant development and response to abiotic stress by determining spliceosome activity specificity. *Plant Cell* **31**, 537–554 (2019).
5. W. G. Fairbrother, R.-F. Yeh, P. A. Sharp, C. B. Burge, Predictive identification of exonic splicing enhancers in human genes. *Science* **297**, 1007–1013 (2002).
6. F. Lejeune, Y. Cavaloc, J. Stevenin, Alternative splicing of intron 3 of the serine/arginine-rich protein 9G8 gene. Identification of flanking exonic splicing enhancers and involvement of 9G8 as a trans-acting factor. *J. Biol. Chem.* **276**, 7850–7858 (2001).
7. J. Ramchatesingh, A. M. Zahler, K. M. Neugebauer, M. B. Roth, T. A. Cooper, A subset of SR proteins activates splicing of the cardiac troponin T alternative exon by direct interactions with an exonic enhancer. *Mol. Cell. Biol.* **15**, 4898–4907 (1995).
8. S. Li, M. Yamada, X. Han, U. Ohler, P. N. Benfey, High-resolution expression map of the Arabidopsis root reveals alternative splicing and lincRNA regulation. *Dev. Cell* **39**, 508–522 (2016).
9. F. Ding *et al.*, Genome-wide analysis of alternative splicing of pre-mRNA under salt stress in Arabidopsis. *BMC Genomics* **15**, 431 (2014).
10. S. A. Filichkin *et al.*, Genome-wide mapping of alternative splicing in Arabidopsis thaliana. *Genome Res.* **20**, 45–58 (2010).
11. Z. Wang *et al.*, ABA signalling is fine-tuned by antagonistic HAB1 variants. *Nat. Commun.* **6**, 8138 (2015).
12. X. Zhan *et al.*, An Arabidopsis PWI and RRM motif-containing protein is critical for pre-mRNA splicing and ABA responses. *Nat. Commun.* **6**, 8139 (2015).
13. H. P. Wu *et al.*, Genome-wide analysis of light-regulated alternative splicing mediated by photoreceptors in Physcomitrella patens. *Genome Biol.* **15**, R10 (2014).
14. E. Petrillo *et al.*, A chloroplast retrograde signal regulates nuclear alternative splicing. *Science* **344**, 427–430 (2014).
15. C. P. G. Calixto *et al.*, Rapid and dynamic alternative splicing impacts the Arabidopsis cold response transcriptome. *Plant Cell* **30**, 1424–1444 (2018).
16. S. A. Filichkin *et al.*, Environmental stresses modulate abundance and timing of alternatively spliced circadian transcripts in Arabidopsis. *Mol. Plant* **8**, 207–227 (2015).
17. S. G. Palusa, G. S. Ali, A. S. N. Reddy, Alternative splicing of pre-mRNAs of Arabidopsis serine/arginine-rich proteins: Regulation by hormones and stresses. *Plant J.* **49**, 1091–1107 (2007).
18. A. S. N. Reddy, G. Shad Ali, Plant serine/arginine-rich proteins: Roles in precursor messenger RNA splicing, plant development, and stress responses. *Wiley Interdiscip. Rev. RNA* **2**, 875–889 (2011).
19. S. de la Fuente van Bentem *et al.*, Phosphoproteomics reveals extensive in vivo phosphorylation of Arabidopsis proteins involved in RNA metabolism. *Nucleic Acids Res.* **34**, 3267–3278 (2006).
20. D. Xing, Y. Wang, M. Hamilton, A. Ben-Hur, A. S. N. Reddy, Transcriptome-wide identification of RNA targets of Arabidopsis SERINE/ARGININE-RICH45 uncovers the unexpected roles of this RNA binding protein in RNA processing. *Plant Cell* **27**, 3294–3308 (2015).

21. S. R. Cutler, P. L. Rodriguez, R. R. Finkelstein, S. R. Abrams, "Abscisic acid: Emergence of a core signaling network" in *Annual Review of Plant Biology*, S. Merchant, W. R. Briggs, D. Ort, Eds. (2010), vol. 61, pp. 651–679.

22. A. S. Raghavendra, V. K. Gonugunta, A. Christmann, E. Grill, ABA perception and signalling. *Trends Plant Sci.* **15**, 395–401 (2010).

23. M. M. Wong et al., Phosphoproteomics of *Arabidopsis* Highly ABA-Induced1 identifies AT-Hook-Like10 phosphorylation required for stress growth regulation. *Proc. Natl. Acad. Sci. U.S.A.* **116**, 2354–2363 (2019).

24. G. B. Bhaskara, T. T. Nguyen, P. E. Verslues, Unique drought resistance functions of the highly ABA-induced clade A protein phosphatase 2Cs. *Plant Physiol.* **160**, 379–395 (2012).

25. R. Antoni et al., Selective inhibition of clade A phosphatases type 2C by PYR/PYL/RCAR abscisic acid receptors. *Plant Physiol.* **158**, 970–980 (2012).

26. S. Savaldi-Goldstein, G. Sessa, R. Fluhr, The ethylene-inducible PK12 kinase mediates the phosphorylation of SR splicing factors. *Plant J.* **21**, 91–96 (2000).

27. S. de la Fuente van Bentem et al., Site-specific phosphorylation profiling of Arabidopsis proteins by mass spectrometry and peptide chip analysis. *J. Proteome Res.* **7**, 2458–2470 (2008).

28. Z. Yang et al., Stable isotope metabolic labeling-based quantitative phosphoproteomic analysis of Arabidopsis mutants reveals ethylene-regulated time-dependent phosphoproteins and putative substrates of constitutive triple response 1 kinase. *Mol. Cell. Proteomics* **12**, 3559–3582 (2013).

29. X. N. Zhang, S. M. Mount, Two alternatively spliced isoforms of the Arabidopsis SR45 protein have distinct roles during normal plant development. *Plant Physiol.* **150**, 1450–1458 (2009).

30. M. N. Kumar, Y. F. Hsieh, P. E. Verslues, At14a-Like1 participates in membrane-associated mechanisms promoting growth during drought in Arabidopsis thaliana. *Proc. Natl. Acad. Sci. U.S.A.* **112**, 10545–10550 (2015).

31. C. Grefen, M. R. Blatt, A 2in1 cloning system enables ratiometric bimolecular fluorescence complementation (rBiFC). *Biotechniques* **53**, 311–314 (2012).

32. G. B. Bhaskara, T. N. Wen, T. T. Nguyen, P. E. Verslues, Protein phosphatase 2Cs and *microtubule-associated stress protein 1* control microtubule stability, plant growth, and drought response. *Plant Cell* **29**, 169–191 (2017).

33. C. Zorzatto et al., NIK1-mediated translation suppression functions as a plant antiviral immunity mechanism. *Nature* **520**, 679–682 (2015).

34. P. Durek et al., PhosPhAt: The Arabidopsis thaliana phosphorylation site database. An update. *Nucleic Acids Res.* **38** (suppl. 1), D828–D834 (2010).

35. E. Roitinger et al., Quantitative phosphoproteomics of the ataxia telangiectasia-mutated (ATM) and ataxia telangiectasia-mutated and rad3-related (ATR) dependent DNA damage response in Arabidopsis thaliana. *Mol. Cell. Proteomics* **14**, 556–571 (2015).

36. Z. J. Lorković, J. Hilscher, A. Barta, Co-localisation studies of Arabidopsis SR splicing factors reveal different types of speckles in plant cell nuclei. *Exp. Cell Res.* **314**, 3175–3186 (2008).

37. T. Kanno, W. D. Lin, C. L. Chang, M. Matzke, A. J. M. Matzke, A genetic screen identifies PRP18a, a putative second step splicing factor important for alternative splicing and a normal phenotype in *Arabidopsis thaliana*. *G3 (Bethesda)* **8**, 1367–1377 (2018).

38. W. Li, W. D. Lin, P. Ray, P. Lan, W. Schmidt, Genome-wide detection of condition-sensitive alternative splicing in Arabidopsis roots. *Plant Physiol.* **162**, 1750–1763 (2013).

39. K. D. Raczynska et al., Involvement of the nuclear cap-binding protein complex in alternative splicing in Arabidopsis thaliana. *Nucleic Acids Res.* **38**, 265–278 (2010).

40. G. Wei et al., Position-specific intron retention is mediated by the histone methyltransferase SDG725. *BMC Biol.* **16**, 44 (2018).

41. M. Kalyna et al., Alternative splicing and nonsense-mediated decay modulate expression of important regulatory genes in Arabidopsis. *Nucleic Acids Res.* **40**, 2454–2469 (2012).

42. Z. Wu et al., RNA binding proteins RZ-1B and RZ-1C play critical roles in regulating pre-mRNA splicing and gene expression during development in Arabidopsis. *Plant Cell* **28**, 55–73 (2016).

43. Q. Yan, X. Xia, Z. Sun, Y. Fang, Depletion of Arabidopsis SC35 and SC35-like serine/arginine-rich proteins affects the transcription and splicing of a subset of genes. *PLoS Genet.* **13**, e1006663 (2017).

44. L. A. Boyer, R. R. Latek, C. L. Peterson, The SANT domain: A unique histone-tail-binding module? *Nat. Rev. Mol. Cell Biol.* **5**, 158–163 (2004).

45. Y. J. Kim et al., POWERDRESS and HDA9 interact and promote histone H3 deacetylation at specific genomic sites in Arabidopsis. *Proc. Natl. Acad. Sci. U.S.A.* **113**, 14858–14863 (2016).

46. C. He et al., High-resolution mapping of RNA-binding regions in the nuclear proteome of embryonic stem cells. *Mol. Cell* **64**, 416–430 (2016).

47. J. Yang et al., The I-TASSER suite: Protein structure and function prediction. *Nat. Methods* **12**, 7–8 (2015).

48. M. Golovkin, A. S. N. Reddy, The plant U1 small nuclear ribonucleoprotein particle 70K protein interacts with two novel serine/arginine-rich proteins. *Plant Cell* **10**, 1637–1648 (1998).

49. S. Lopato, R. Gattoni, G. Fabini, J. Stevenin, A. Barta, A novel family of plant splicing factors with a Zn knuckle motif: Examination of RNA binding and splicing activities. *Plant Mol. Biol.* **39**, 761–773 (1999).

50. V. Tillemans, I. Leponce, G. Rausin, L. Dispa, P. Motte, Insights into nuclear organization in plants as revealed by the dynamic distribution of Arabidopsis SR splicing factors. *Plant Cell* **18**, 3218–3234 (2006).

51. G. S. Ali, A. S. N. Reddy, ATP, phosphorylation and transcription regulate the mobility of plant splicing factors. *J. Cell Sci.* **119**, 3527–3538 (2006).

52. N. Stankovic et al., Dynamic distribution and interaction of the Arabidopsis SRSF1 subfamily splicing factors. *Plant Physiol.* **170**, 1000–1013 (2016).

53. P. Wang et al., Quantitative phosphoproteomics identifies SnRK2 protein kinase substrates and reveals the effectors of abscisic acid action. *Proc. Natl. Acad. Sci. U.S.A.* **110**, 11205–11210 (2013).

54. T. Umezawa et al., Genetics and phosphoproteomics reveal a protein phosphorylation network in the abscisic acid signaling pathway in Arabidopsis thaliana. *Sci. Signal.* **6**, rs8 (2013).

55. Y. Ling et al., Thermopriming triggers splicing memory in Arabidopsis. *J. Exp. Bot.* **69**, 2659–2675 (2018).

56. M. J. Kim et al., Controlled nuclear import of the transcription factor NTL6 reveals a cytoplasmic role of SnRK2.8 in the drought-stress response. *Biochem. J.* **448**, 353–363 (2012).

57. Z. T. Yang et al., A plasma membrane-tethered transcription factor, NAC062/ANAC062/NTL6, mediates the unfolded protein response in Arabidopsis. *Plant J.* **79**, 1033–1043 (2014).

58. S. R. Thatcher et al., Genome-wide analysis of alternative splicing during development and drought stress in maize. *Plant Physiol.* **170**, 586–599 (2016).

59. P. Lan, W. Li, W. D. Lin, S. Santi, W. Schmidt, Mapping gene activity of Arabidopsis root hairs. *Genome Biol.* **14**, R67 (2013).

PLANT BIOLOGY